The EMBO Journal (2012) 31, 4191–4203 | © 2012 European Molecular Biology Organization | All Rights Reserved 0261-4189/12
www.embojournal.org

THE EMBO JOURNAL

The exomer cargo adaptor structure reveals a novel GTPase-binding domain

Jon E Paczkowski[1], Brian C Richardson[1], Amanda M Strassner and J Christopher Fromme*

Department of Molecular Biology and Genetics, Weill Institute for Cell and Molecular Biology, Cornell University, Ithaca, NY, USA

Cargo adaptors control intracellular trafficking of transmembrane proteins by sorting them into membrane transport carriers. The COPI, COPII, and clathrin cargo adaptors are structurally well characterized, but other cargo adaptors remain poorly understood. Exomer is a specialized cargo adaptor that sorts specific proteins into *trans*-Golgi network (TGN)-derived vesicles in response to cellular signals. Exomer is recruited to the TGN by the Arf1 GTPase, a universally conserved trafficking regulator. Here, we report the crystal structure of a tetrameric exomer complex composed of two copies each of the Chs5 and Chs6 subunits. The structure reveals the FN3 and BRCT domains of Chs5, which together we refer to as the FBE domain (FN3–BRCT of exomer), project from the exomer core complex. The overall architecture of the FBE domain is reminiscent of the appendage domains of other cargo adaptors, although it exhibits a distinct topology. In contrast to appendage domains, which bind accessory factors, we show that the primary role of the FBE domain is to bind Arf1 for recruitment of exomer to membranes.

The EMBO Journal (2012) **31,** 4191–4203. doi:10.1038/emboj.2012.268; Published online 21 September 2012
Subject Categories: membranes & transport; structural biology
Keywords: Arf1; cargo adaptor; GTPase; membrane trafficking; *trans*-Golgi network

Introduction

Eukaryotic cells control the subcellular localization of integral membrane proteins primarily through protein complexes that bind to the cytosolic domains of transmembrane cargo proteins to mediate trafficking of the cargo towards the target compartment (Schekman and Orci, 1996; Bonifacino and Glick, 2004). Many of these cargo adaptor complexes are recruited from the cytoplasm to the membrane surface of the donor compartment by activated GTPases of the Arf superfamily (Donaldson and Jackson, 2011). Trafficking adaptors usually function as integral components of vesicle coats, sorting cargo into nascent membrane vesicles and tubules and contributing to the morphogenesis of these transport carriers (Schekman and Orci, 1996; Bonifacino and Lippincott-Schwartz, 2003).

Trafficking of cargo from the *trans*-Golgi network (TGN) is particularly complex, requiring several different cargo adaptors to sort cargo towards a host of different destinations, including the plasma membrane (PM) and various compartments of the endolysosomal system (De Matteis and Luini, 2008; Glick and Nakano, 2009). Much progress has been made in understanding the structural basis for the function of clathrin-dependent cargo adaptors and the COPI and COPII vesicle coats (Owen *et al*, 1999; Bi *et al*, 2002; Collins *et al*, 2002; Mossessova *et al*, 2003; Heldwein *et al*, 2004; Edeling *et al*, 2006; Bi *et al*, 2007; Jackson *et al*, 2010; Lee and Goldberg, 2010; Yu *et al*, 2012). However, outside of these well-described systems, comparatively little is known regarding the structural basis for the function of other cargo adaptors.

Exomer is an Arf1 GTPase-dependent protein complex required for trafficking of specific cargo proteins from the TGN to the PM (Sanchatjate and Schekman, 2006; Trautwein *et al*, 2006; Wang *et al*, 2006). Exomer physically interacts with transmembrane cargo proteins that require it for trafficking (Sanchatjate and Schekman, 2006; Barfield *et al*, 2009). The exomer complex decorates membranes but is not sufficient to deform membranes (Wang *et al*, 2006), and is therefore most appropriately categorized as a cargo adaptor, if not a *bona fide* vesicle coat. Traffic of exomer-dependent cargo is highly regulated: the model cargo Chs3 is trafficked from the TGN to the PM by exomer in a cell-cycle-dependent manner, despite being expressed continuously throughout the cell-cycle (Chuang and Schekman, 1996; Santos and Snyder, 1997; Zanolari *et al*, 2011), and the exomer cargo Fus1 is targeted to the PM in response to pheromone signalling (Santos *et al*, 1997; Santos and Snyder, 2003; Barfield *et al*, 2009). It remains unknown how exomer-dependent trafficking of these cargos is controlled by these signalling pathways.

The exomer complex consists of the Chs5 protein and four mutually paralogous proteins termed the ChAPs (for Chs5 and Arf1 binding Proteins): Chs6, Bud7, Bch1, and Bch2 (Trautwein *et al*, 2006). These five proteins interact *in vivo* (Trautwein *et al*, 2006) and co-purify as a complex (Sanchatjate and Schekman, 2006). The *CHS5* and *CHS6* genes are named based on their role in cell wall chitin synthesis (Roncero *et al*, 1988; Bulawa, 1992; Choi *et al*, 1994), and are required for trafficking the Chs3 chitin synthase to the PM (Santos and Snyder, 1997; Ziman *et al*, 1998). *BUD7* was originally identified in a screen for genes affecting bud-site selection (Zahner *et al*, 1996); *BCH1* and *BCH2* are named for their homology (*BUD7* and *CHS6* homologues). The contrast of specific phenotypes of individual ChAP deletion mutants with the overlapping phenotypes of *chs5*Δ mutants suggests that ChAPs act as cargo-specific adaptors and Chs5 serves a more general, perhaps structural, role in exomer function (Trautwein *et al*, 2006).

*Corresponding author. Department of Molecular Biology and Genetics, Weill Institute for Cell and Molecular Biology, Cornell University, 457 Weill Hall, Ithaca, NY 14853, USA. Tel.: +1 607 255 1016; Fax: +1 607 255 5961; E-mail: jcf14@cornell.edu
[1]These authors contributed equally to this work

Received: 5 July 2012; accepted: 30 August 2012; published online: 21 September 2012

Subunits of the exomer complex have been identified in a diverse set of single-celled eukaryotes (Trautwein *et al*, 2006), but no clear homologues have been found in metazoans. Nevertheless, exomer serves as an important model system for understanding the regulation of cargo trafficking from the TGN in higher eukaryotes, based on the tightly regulated trafficking of its cargos and the functional interaction between exomer and other trafficking machinery that is conserved in metazoans, including the Arf1 GTPase, the TGN-localized Rab proteins Ypt31/32 (Rab11 homologues), and the Myosin V motor Myo2 (Santos and Snyder, 1997; Ortiz and Novick, 2006; Trautwein *et al*, 2006).

To gain insight into exomer function we determined the structure of a functional exomer complex. This structure, with accompanying functional studies, establishes the molecular architecture of the complex and the domains involved in membrane recruitment. The structure reveals that the tandem FN3–BRCT domain of Chs5 projects from the exomer core complex. We demonstrate that this domain binds directly to Arf1, and is required for stable recruitment of exomer to membranes *in vitro* and *in vivo*.

Results

The structure of a functional exomer complex

We first determined that residues 1–274 represent the minimal functional fragment of Chs5, based on proper *in vivo* trafficking of Chs3–GFP (Figure 1A and B; Supplementary Figure 1). This finding is consistent with a recent report, demonstrating that the C-terminus of Chs5 is dispensable for exomer function (Martin-Garcia *et al*, 2011). On the basis of this result, we determined the crystal structure of a functional exomer complex consisting of Chs6 and residues 1–299 of Chs5 (Chs5/6 exomer complex). The final model (Figure 1C; Supplementary Figures 2 and 3A; Supplementary Movie 1) was refined against a 2.75 Å native data set resulting in good statistics (Supplementary Table 1). The asymmetric unit contains one molecule of Chs6 in complex with one molecule of Chs5(1–299).

Chs5 is an elongated protein with four small domains (Figure 1D; Supplementary Figure 3B). From N-terminus to C-terminus, it consists of an anti-parallel β-sheet motif, a long α-helix, a fibronectin 3 (FN3) domain, and a BRCA1 C-terminus (BRCT) domain. The linker between the α-helix and the FN3 domain may be flexible, as it consists of a glycine followed by three hydrophilic residues lacking regular secondary structure. As a result of this architecture, the FN3 and BRCT domains project away from the bulk of the complex. For simplicity, we refer to this fragment of Chs5 as the FBE domain (FN3–BRCT of exomer).

Chs6 forms a large ring structure (Figure 1E) and comprises mainly α-helices, including several tetratricopeptide repeat (TPR) motifs, and a single five-stranded mixed β-sheet. The topology of Chs6 is complex, with the polypeptide chain meandering back and forth about the ring structure, forming a single structural domain of ~700 residues (Supplementary Figure 2F). Although there is some resemblance to the helical solenoid structures found in other trafficking and membrane sculpting proteins (Brohawn *et al*, 2008), the fold of Chs6 is unique, as it only shares a resemblance to known structures at the level of the TPR motifs that are scattered throughout the domain (Supplementary Table 2).

Surprisingly, a solvent channel lies at the centre of the Chs6 ring (Figure 1E, inset). Within this solvent channel there is a cleft containing electron density unattributable to any protein atoms. We could reasonably model a molecule of HEPES, a component of the buffers used for purification and crystallization, into the electron density at this site.

The Chs5–Chs6 interaction interface

Chs5 binds to Chs6 through two different motifs (Figure 2A). The long α-helix of Chs5 (residues 54–76) binds to the surface of Chs6 primarily by interacting with a single long α-helix in Chs6 (residues 300–321) otherwise orphaned in the middle of several TPR repeats. This helix in Chs6 runs anti-parallel to the long helix of Chs5, and extensive hydrophobic and electrostatic interactions occur between the two helices (Figure 2B), similar to the helix–helix interactions of TPR motifs. Thus, these two helices together form an intermolecular TPR-like motif. Additionally, the small β-sheet at the N-terminus of Chs5 packs against a concave hydrophobic surface of Chs6, adjacent to where the Chs5 α-helix binds. The two surfaces of Chs6 contacting Chs5 represent the most highly conserved regions of ChAP protein surface, as determined from sequence alignments generated using all four ChAP proteins (Figure 2A).

We used structure-based mutagenesis to test the importance of these regions for the Chs5–Chs6 interaction. We first found that a Chs5 construct lacking the N-terminal 50 amino acids comprising the β-sheet domain formed a robust interaction with Chs6 and with another ChAP, Bch1, when co-expressed in *Escherichia coli* (Supplementary Figure 4A and B), indicating that this region of Chs5 is dispensable for the Chs5–ChAP interaction. In contrast, introducing a two-residue mutation in the long α-helix of Chs5, F63E/Q67E, disrupted the Chs5–Chs6 interaction (Figure 2C). We note that neither the F63E nor the Q67E single mutants disrupted the Chs5–Chs6 interaction, suggesting that this interface is stable enough to tolerate moderate perturbation. We found that introduction of a mutation in the Chs6 α-helix that contacts the Chs5 α-helix, I305R, also destabilized the Chs5–Chs6 interaction (Figure 2D).

We found that disrupting the Chs5–Chs6 interaction compromised exomer function *in vivo*, as monitored by cellular sensitivity to the toxin calcofluor white conferred by exomer-mediated trafficking of Chs3 to the PM (Valdivieso *et al*, 1991; Santos and Snyder, 1997). Consistent with the *in vitro* interaction results, cells expressing either the F63E or Q67E Chs5 single mutants were sensitive to calcofluor, whereas cells expressing the F63E/Q67E Chs5 double mutant were as resistant to calcofluor as *chs5*Δ cells (Figure 2E), despite this mutant being expressed at a level similar to that of wild-type Chs5 (Supplementary Figure 4C). We then examined the localization of Chs6–GFP in cells expressing these Chs5 mutants. Correlating with the results of the calcofluor sensitivity and *in vitro* interaction assays, we found that Chs6–GFP was properly localized to the TGN in cells expressing either the F63E or Q67E single mutant versions of Chs5, but was severely mislocalized in the F63E/Q67E Chs5 mutant, similar to its localization in *chs5*Δ cells (Figure 2F). This result confirms a previous finding that Chs6 requires Chs5 in order to localize to the TGN (Trautwein *et al*, 2006).

Taken together, these results demonstrate that the α-helical Chs5–Chs6 interface observed in the crystal structure, which

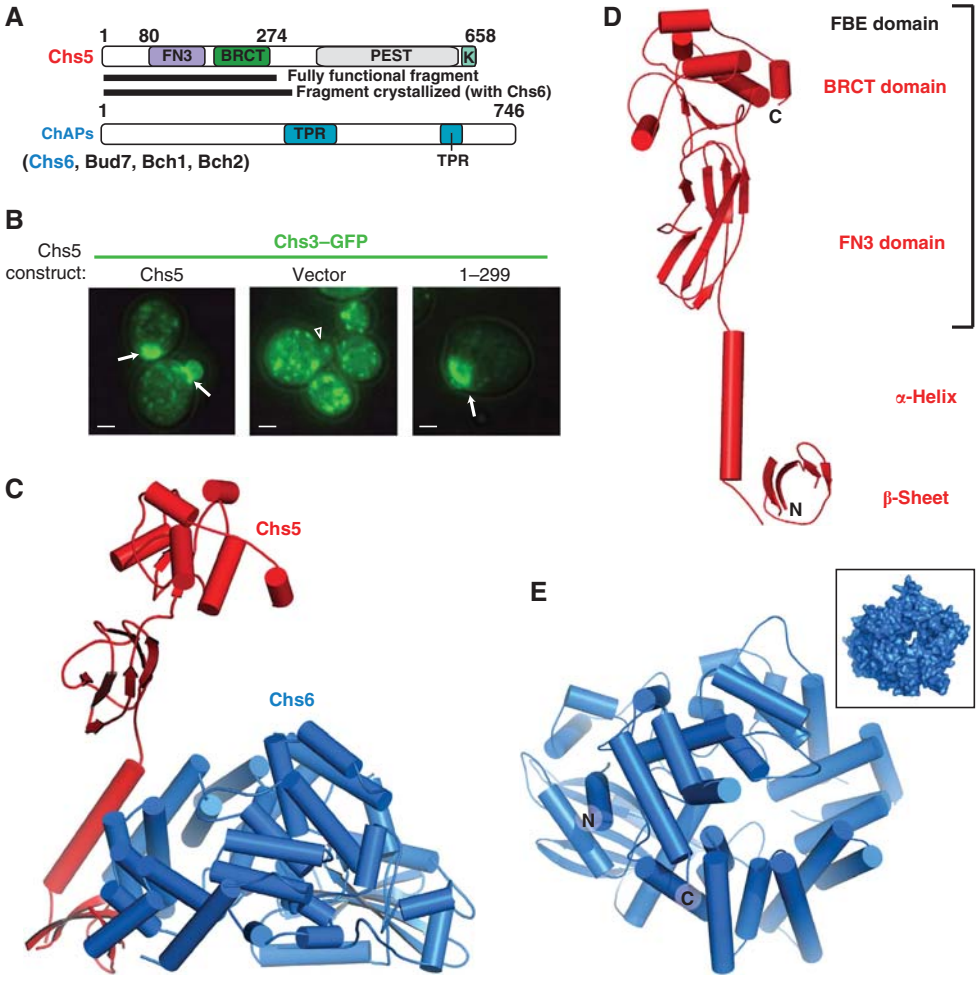

Figure 1 Molecular architecture of the Chs5/6 exomer heterodimer. (**A**) Schematic of exomer subunit constructs used, with domains and motifs identified by searching the SMART and TPRpred databases. Exomer complexes form through association of Chs5 with one or more of the ChAPs (Chs6, Bud7, Bch1, and Bch2). (**B**) Chs3–GFP localization of yeast cells expressing residues 1–299 of Chs5 phenocopies that of cells expressing full-length Chs5 (residues 1–658). Plasmids expressing Chs5 constructs or empty vector were introduced into *chs5*Δ Chs3–GFP cells (yeast strain CFY264). Images show a single focal plane, with GFP and DIC channels merged. Arrows indicate proper localization of Chs3–GFP to incipient bud sites and the mother-bud neck of very small buds. Arrowhead indicates lack of proper localization in cells lacking functional Chs5. Scale bar, 2 μm. (**C**) The structure of the Chs5(1–299)/Chs6 heterodimer asymmetric unit, shown as a ribbon diagram. Chs5 is red and Chs6 is blue. (**D**) Ribbon diagram of the Chs5(1–299) structure, indicating the four different structural motifs. (**E**) Ribbon diagram of the Chs6 structure, from a top–down perspective relative to (**C**). Inset shows the same perspective as a surface diagram to visualize the solvent channel in Chs6. See also Supplementary Movie 1.

buries 817 Å^2 of solvent accessible surface, is functionally relevant *in vivo*.

Exomer is a heterotetramer

Previous analysis of the exomer complex in detergent-solubilized cell extracts found that immunoprecipitation of Chs5 or of any single ChAP resulted in co-immunoprecipitation of all four ChAP proteins (Sanchatjate and Schekman, 2006; Trautwein *et al*, 2006). Size analysis of solubilized extracts (Sanchatjate and Schekman, 2006) and of recombinant exomer subunits expressed in insect cells (Wang *et al*, 2006) also suggested that exomer likely exists as a multimeric complex.

We performed sedimentation velocity and Stokes radius analysis (Figure 3A and B) to determine that the recombinant Chs5/6 exomer complex is a heterotetramer, based on a native molecular weight of 205 kDa (two copies of Chs6 and two copies of Chs5(1–299) have an expected molecular weight of 240 kDa). Complementary analysis by a different technique, multiangle light scattering (MALS) (De *et al*, 2010), yielded a similar value of 195 ± 10 kDa (Supplementary Figure 5A), confirming this result (we note that the experimentally determined molecular weight may be slightly lower than expected due to partial proteolysis or complex dissociation during production and purification of the recombinant proteins). A heterotetramer is also consistent with an experiment, demonstrating that exomer complexes isolated from cells using epitope-tagged Chs6 contain the other ChAPs in significantly lower abundance (Sanchatjate and Schekman, 2006).

We found that deletion of the N-terminal β-sheet of Chs5 reduced the Stokes radius of the Chs5–Chs6 complex by 21% (Figure 3B), corresponding to a 50% reduction in the hydrodynamic volume of the complex. In addition, this construct exhibited a native molecular weight of 117 kDa as determined by MALS (Supplementary Figure 5B), closely matching the 115 kDa calculated molecular weight of a single

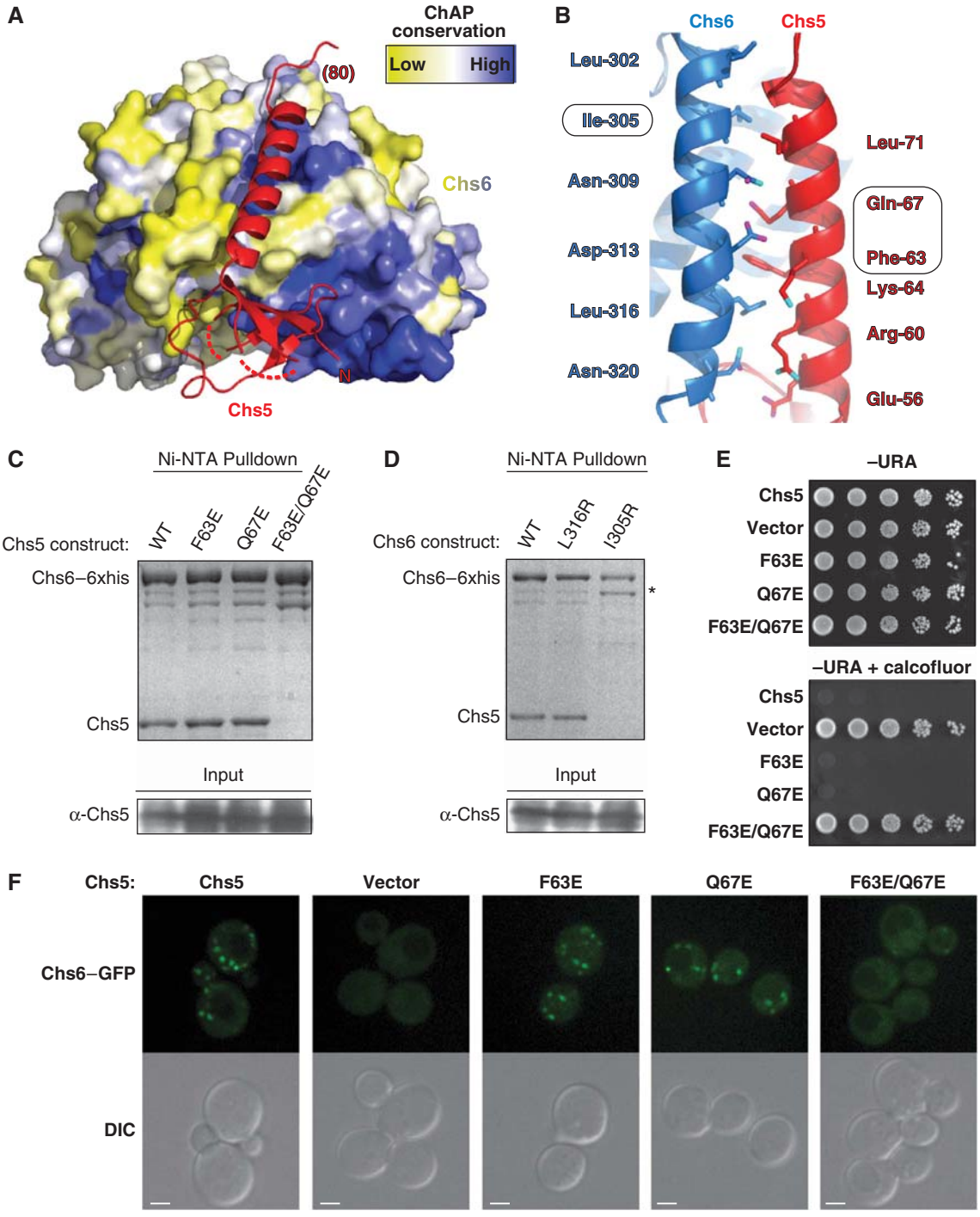

Figure 2 The Chs5–Chs6 interaction interface. (**A**) Residues 1–80 of Chs5(1–299) are shown as a red ribbon. Chs6 is coloured by conservation based on a sequence alignment of the four *S. cerevisiae* ChAP proteins (Chs6, Bud7, Bch1, Bch2). Blue indicates residues that are most conserved, yellow indicates residues that are least conserved, according to a normalized conservation score calculated by ConSurf (Ashkenazy *et al*, 2010). (**B**) Close-up view of the interaction of the Chs5 α-helix (residues 50–74) with Chs6. Chs5 is red and Chs6 is blue. The outlined residue numbers denote the positions that disrupt the interaction when mutated, as shown in parts (**C**, **D**). (**C**) Purification from *E. coli* of recombinant exomer complexes with mutations in the Chs5 subunit. Purified samples were loaded after normalizing for Chs6 levels. The immunoblot indicates the relative expression levels of the mutant Chs5 subunits in the *E. coli* lysates, as detected by anti-Chs5. (**D**) Purification of exomer complexes with mutations in the Chs6 subunit, performed as in (**C**). The asterisk denotes a resin-binding *E. coli* contaminant that is more prominent in the I305R mutant. (**E**) Plasmids expressing Myc-tagged Chs5 constructs were introduced into *chs5*Δ cells (CFY857). Serial dilutions were spotted onto the indicated media and imaged after 2 days of growth at 30°C. Calcofluor white was used at 50 μg/ml. Cells with disrupted Chs3 trafficking (i.e., exomer mutants) are able to grow in the presence of this toxin. (**F**) Imaging of chromosomal Chs6–GFP in *chs5*Δ cells (CFY857) expressing plasmid borne Myc-tagged Chs5 constructs. Single confocal sections are shown. Scale bar, 2 μm. Figure source data can be found with the Supplementary data.

Chs5(51–299)/Chs6 heterodimer. Deletion of residues 1–50 of Chs5 did not disrupt the Chs5–Chs6 interaction (Supplementary Figure 4A). Therefore, this motif mediates formation of an exomer heterotetramer via dimerization of two Chs5/6 heterodimers. Importantly, loss of this 50-residue N-terminal homodimerization motif abrogated exomer func-

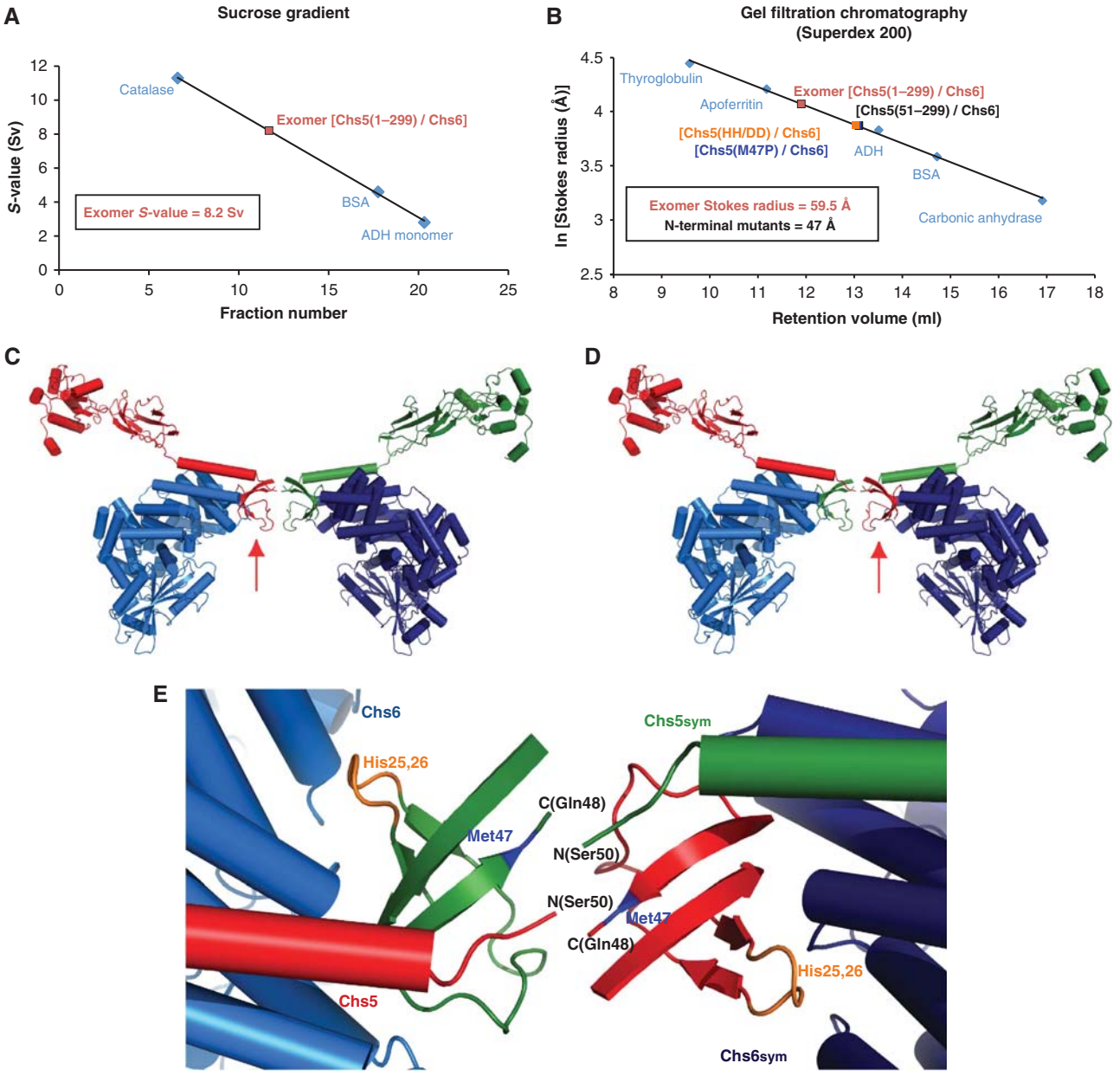

Figure 3 The Chs5 N-terminus mediates formation of the exomer heterotetramer. (**A**) Sedimentation velocity analysis, using sedimentation on a sucrose gradient relative to standards to determine the *S*-value of the Chs5(1–299)/Chs6 exomer complex. (**B**) Stokes radius analysis, using retention volume on a Superdex 200 gel filtration column. (**C**) View of a crystal-packing interaction that relates two asymmetric units via homodimeric interaction of the Chs5 N-terminus. The symmetry mate is coloured dark blue (Chs6) and green (Chs5). In both (**C**, **D**), the red arrow denotes the Chs5 N-terminus belonging to the heterodimer on the left. (**D**) Domain swap model of the heterotetramer, with colouring otherwise as in (**C**). Note the red arrow now points to the Chs5 N-terminus in the symmetry-related position. (**E**) Close-up view of the crystal-packing interface of the domain swap model, demonstrating the lack of continuity in the model between the N-terminus (residues 1–50) and the long α-helix of Chs5 (starting after residue 50). The loop expected to contain His25 and His26 is coloured orange (both of these residues are mutated to Asp in Chs5(HH/DD)/Chs6). The modelled position of Met47 (site of the M47P mutation) in the polypeptide is coloured blue. See also Supplementary Movie 2.

tion *in vivo* (Supplementary Figure 1C). Chs5-mediated heterotetramerization is consistent with the finding that ChAP–ChAP interactions were lost in *chs5*Δ mutant cells, but not in cells lacking individual ChAP genes (Sanchatjate and Schekman, 2006).

The observation that exomer is a tetramer is at odds with the presence of only a single Chs5/6 pair in the crystal asymmetric unit. Examining crystallographic symmetry revealed that exomer packs in a tight hexamer of heterodimers mediated by Chs6–Chs6 crystal contacts (Supplementary Figure 5G). Within this hexamer, two-fold crystallographic axes relate pairs of Chs5/6 heterodimers contacting each other by their Chs5 N-termini (Figure 3C), as would be expected from the biochemical data, indicating that this domain mediates formation of the tetramer. The electron density of the Chs5 N-terminal β-sheets is quite weak, consistent with partial disruption of the dimeric interaction by the extensive crystal contacts, resulting from the hexameric packing. MALS analysis of exomer in the crystallization solution indicated a size of 191 kDa (Supplementary Figure 5C),

consistent with a heterotetramer; therefore, the weak electron density is unlikely to be a result of salt or buffer-dependent disruption of the tetramer. Thus, the heterotetrameric exomer complex can be modelled via this crystal-packing interaction (Figure 3C), though the electron density does not allow modelling of side chains in the Chs5 N-terminal domain. Therefore, precise residue numbers cannot be assigned to this region of the model beyond those indicated by secondary structure prediction (Supplementary Figure 4D).

We were initially concerned that the Chs5–Chs5 contact surface area is less than expected for a stable interaction. We therefore considered an alternative model involving domain swapping, in which neighbouring N-termini reach across each other to bind *in trans* with the opposing Chs6 molecule (Figure 3D and E; Supplementary Movie 2). Domain swapping would account for tetramerization despite the low Chs5–Chs5 surface contact area, because the tetramer would be stabilized by the additional interaction of the Chs5 N-terminus with the opposite Chs6 molecule. The domain swap model is consistent with our finding that deletion of the Chs5 N-terminus disrupted tetramerization (Figure 3B; Supplementary Figure 5B), but did not disrupt the Chs5–Chs6 interaction (Supplementary Figure 4A); this model is also consistent with an alternative interpretation of the asymmetric unit (Supplementary Figure 3).

To further test the domain swap model, we generated two point mutants in the N-terminus of Chs5 based on the alignment of predicted secondary structure to the observed main chain density. One mutation, H25D/H26D, we predict to lie in a loop contacting a conserved surface of Chs6; the other mutation, M47P, we predict to disrupt the β-strand mediating the hypothesized domain swap (Figure 3E). Both mutants disrupted exomer tetramerization without disrupting the Chs5/Chs6 interaction (Supplementary Figure 5D–F). These experiments are consistent with the domain swap model; however, we cannot rule out the alternative configuration. Further structural studies are needed to establish the precise atomic details of the tetramerization interface.

Our finding that exomer is a heterotetramer is consistent with previous studies (Sanchatjate and Schekman, 2006; Trautwein *et al*, 2006; Wang *et al*, 2006), and implies that both mixed exomer heterotetramers (containing two Chs5 molecules and two different ChAPs) and homogeneous exomer heterotetramers (containing two Chs5 molecules and two identical ChAPs) likely exist *in vivo*.

The FBE domain resembles appendage domains

Although sharing no obvious sequence homology, the structure of the FBE domain of Chs5 (residues 77–285) resembles 'appendage' domains found in the clathrin adaptors and COPI (Figure 4). The appendage domains of these cargo adaptors consist of either an N-terminal β-sandwich subdomain and a C-terminal mixed α/β 'platform' subdomain, or just the β-sandwich domain (Owen *et al*, 1999, 2000; Kent *et al*, 2002; Collins *et al*, 2003; Hoffman *et al*, 2003). The FBE domain also consists of an N-terminal β-sandwich subdomain and a C-terminal mixed α/β subdomain. The precise folds are not identical: the β-sandwich of the clathrin adaptors and COPI consists of an immunoglobulin-like fold, whereas the β-sandwich of Chs5 is a similar but distinct FN3 fold, and the mixed α/β subdomain of Chs5 is a BRCT fold, unlike the platform subdomain of the clathrin adaptor and COPI appendages, which exhibits a much larger β-sheet. The relative orientation of the two subdomains are quite similar in Chs5, the clathrin adaptors and COPI. In particular, an α-helix is projected from the distal end of the FBE domain, and the α2, β2, and γ-COP appendage domains (located at the top of orientation shown in Figure 4). We note that despite the overall resemblance, the FBE domain cannot be classified as a true appendage domain, and indeed has a function distinct from that of appendage domains, as we demonstrate below.

Chs6 binds directly to membranes and the FBE domain binds directly to Arf1

Previous studies found that exomer localization to the TGN *in vivo* and robust recruitment to liposome membranes *in vitro* depend upon Arf1 (Wang *et al*, 2006). Chs5 localizes correctly to the TGN in the absence of any ChAP proteins (Trautwein *et al*, 2006), indicating that the primary determinants of exomer localization and Arf1 interaction lie within the Chs5 subunit.

To determine which domain(s) of Chs5 mediate the exomer–Arf1 interaction, we used the crystal structure to design and generate stable, well-behaved truncation constructs, based on the observation that the three regions of Chs5 (N-terminus, helix, and FBE) are structurally independent and separated by short linkers (Figure 1D). We assessed the ability of these constructs to be recruited to liposome membranes by Arf1 using a liposome flotation assay (Wang *et al*, 2006). We confirmed that the Chs5/6 complex was stably recruited to liposomes in an Arf1–GTP-dependent manner (Figure 5A). In contrast, the 'ΔN' [Chs5(51–299)/Chs6] construct was more weakly bound to membranes, indicating loss of the robust interaction with Arf1–GTP. The 'core' [Chs5(1–80)/Chs6] exomer complex was not detected in the membrane-bound fractions. These results indicate that both the N-terminal and FBE domains of Chs5 play key roles in stable recruitment of exomer to the membrane surface by Arf1.

A previous study found that exomer can bind to membranes of strong negative charge in an Arf1-independent manner (Wang *et al*, 2006). To assess Arf1-independent membrane association of the truncated Chs5 exomer constructs, we utilized a liposome pelleting assay. Whereas the flotation assay involves transit of liposomes through a protein-free layer of solution within the sucrose gradient, in the pelleting assay liposomes remain in contact with the protein-containing solution during pelleting. Thus, binding equilibria with higher off-rates can be detected by the pelleting assay. As pelleting of protein aggregates can complicate the interpretation of liposome pelleting assays, we were careful to analyse the data quantitatively and to subtract any observed background pelleting (see Materials and methods). We found that the Chs5/6 complex bound to liposomes composed of either a TGN-like lipid mix or Folch fraction I lipids (Figure 5B), confirming that Chs5/6 has an affinity for anionic membrane surfaces. Next, we compared the Chs5/6, ΔN, core, and Chs6 constructs to determine which domains of exomer are required for Arf1-independent membrane association. We observed that both Chs6 and the ΔN construct bind membranes, while the Chs5/6 and exomer core constructs exhibited even higher levels of membrane binding (Figure 5C; Supplementary Figure 6A and B). Neither the isolated Chs5 N-terminus nor the isolated FBE domain

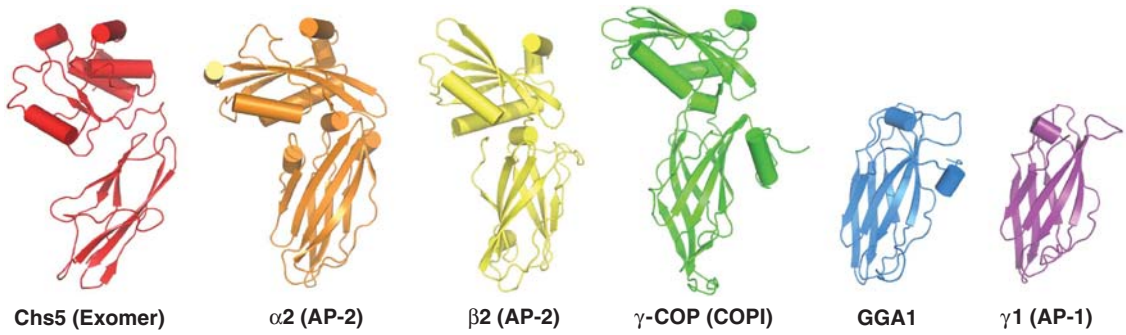

Figure 4 The Chs5 FBE domain resembles appendage domains of other cargo adaptors. Structural resemblance of the Chs5 FBE domain (this work) and the appendage domains of the α2 subunit of AP-2 (PDB: 1B9K) (Owen *et al*, 1999), the β2 subunit of AP-2 (PDB: 1E42) (Owen *et al*, 2000), the γ-COP subunit of COPI (PDB: 1PZD) (Hoffman *et al*, 2003), GGA1 (PDB: 1OM9) (Collins *et al*, 2003), and the γ1 subunit of AP-1 (PDB: 1GYU) (Kent *et al*, 2002).

(purified as GST-fusions) bound to membranes (Figure 5D; Supplementary Figure 6C). These data show that Chs6 binds directly to membranes, and that the Chs5 N-terminus enhances this interaction, likely via dimerization. The results also indicate that the FBE domain is dispensable for Arf1-independent membrane binding.

In light of these data, the results of the flotation assay suggested that the FBE domain was most critical for Arf1-dependent stable membrane binding. We therefore tested whether the FBE domain directly interacted with Arf1, and we observed binding of ΔN17-Arf1 to a GST–FBE domain construct in a pulldown experiment (Figure 5E). We note that both GTP- and GDP-loaded ΔN17-Arf1 bound equally well to the FBE domain construct. This implies that the FBE domain may interact with a surface on Arf1 other than the 'switch' regions, which is classically where effectors bind (with notable exceptions (Saci *et al*, 2011)). This result is addressed further below.

To assess whether Chs6 membrane binding was cooperative with FBE domain Arf1 binding, we used the pelleting assay to investigate membrane association of the ΔN construct in the presence of Arf1. We found that the presence of Arf1 on the liposomes significantly enhanced the binding of the ΔN construct to membranes, whereas Arf1 did not enhance recruitment of the isolated FBE domain or of Chs6 under the conditions tested (Figure 5F; Supplementary Figure 6D). Therefore, the FBE domain cooperates with Chs6 to bind membranes in an Arf1-dependent manner.

Taken together, the Arf1-dependent and Arf1-independent membrane binding studies demonstrate that Chs6 binds to membranes and the FBE domain binds to Arf1. The Chs5 N-terminus increases the affinity of the complex for both membranes and membrane-bound Arf1, likely through dimerization. The data also indicate that each individual interaction (Chs6-membrane and FBE-Arf1) is of relatively low affinity, and it is the combination of both interactions that allows exomer to be recruited to membranes in an Arf1-dependent manner.

Exomer inhibits ArfGAP activity, dependent upon the FBE domain

Some cargo adaptors and vesicle coats modulate GAP activity on their cognate GTPases (Yoshihisa *et al*, 1993; Goldberg, 1999; Antonny *et al*, 2001; Yu *et al*, 2012). Furthermore, the appendage domain of γ-COP interacts directly with ArfGAP (Watson *et al*, 2004; Kliouchnikov *et al*, 2009; Schindler *et al*, 2009). Thus, we tested whether exomer affects the enzymatic activity of Age2, the primary ArfGAP in yeast that localizes and functions exclusively at the TGN (Poon *et al*, 2001). We used an established tryptophan fluorescence assay (Antonny *et al*, 1997) to measure the activity of the Age2 GAP domain on Arf1–GTP bound to liposomes. Under the conditions that we tested (0.5 μM Arf1, 0.5 μM GAP, 0.25 μM exomer construct), we found that both the Chs5/6 complex and the ΔN construct significantly inhibited GAP activity (Figure 6A and B), as might be expected from an Arf1 effector that competes with the GAP for binding to Arf1–GTP. The ΔN-construct did not inhibit GAP activity as strongly as the intact Chs5/6 complex, again, indicating that dimerization by the N-terminus enhances association of exomer with membrane-bound Arf1 through an avidity affect. Neither the core complex nor Chs6 inhibited GAP activity, indicating GAP inhibition relied upon the FBE domain.

ArfGAPs can bind to Arf1 simultaneously with effectors (such as COPI) that bind to the GTPase switch regions. This is because the ArfGAP domain contacts only the periphery of the switch regions, instead binding primarily near the guanine binding pocket, distal to the membrane surface (Ismail *et al*, 2010; Yu *et al*, 2012). This arrangement allows COPI to stimulate ArfGAP activity, likely by serving as a scaffold to increase encounters between Arf1 and ArfGAP (Yu *et al*, 2012). In contrast, exomer inhibits ArfGAP activity, dependent on the FBE domain. This strongly suggests that the FBE domain and ArfGAP bind to an overlapping surface of Arf1. Importantly, this is consistent with our observation that the FBE domain binds to Arf1 in a nucleotide-independent manner, likely by binding to a non-switch region of Arf1.

Multiple domains cooperate to localize exomer to the TGN

Based on the results of the *in vitro* assays, we predicted that the three major domains of exomer—the Chs5 N-terminus, the FBE domain, and the ChAP subunit—would each play significant roles in localizing exomer to the TGN. To test this prediction, we determined the localization of GFP–Chs5 truncations in *chs5*Δ cells. Proper localization of Chs5 fragments was assayed by examining co-localization with the TGN marker Sec7. As expected, GFP–Chs5(1–299) co-localized extensively with Sec7 and its localization pattern was

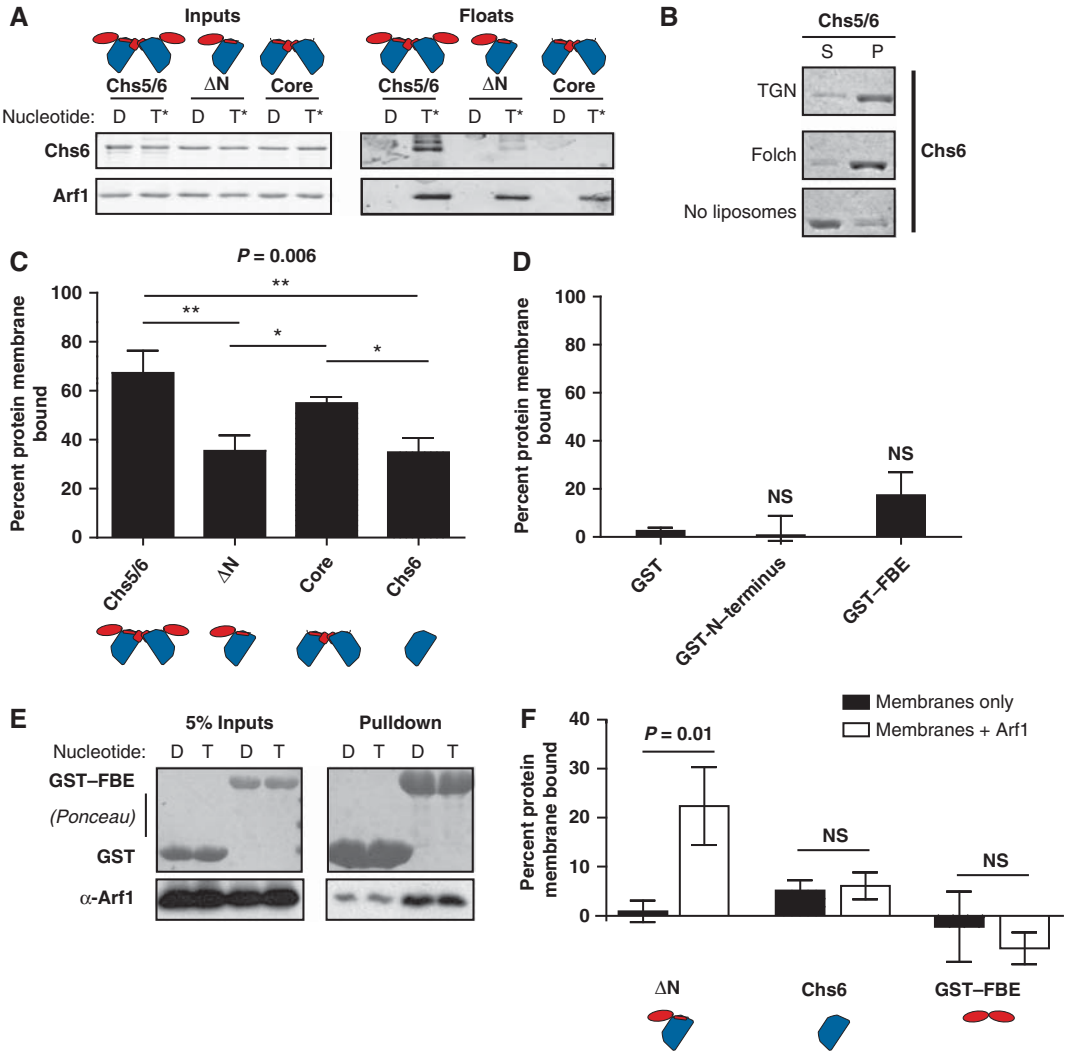

Figure 5 Chs6 binds to membranes and the FBE domain binds to Arf1 to recruit exomer to membranes. (**A**) Liposome flotation assay comparing Arf1-dependent membrane binding of different exomer constructs. 'T*' denotes Arf1 bound to GMPPNP, 'D' denotes Arf1 bound to GDP. For simplicity, only the Chs6 protein band is shown for each construct; this is the band that was used for subsequent quantification. (**B**) Liposome pelleting assay measuring Arf1-independent membrane binding. 'TGN', TGN-like liposomes, 'Folch', Folch fraction I liposomes. 'S', supernatant fractions, 'P', pellet fractions. (**C**) Quantification of Arf1-independent membrane binding. Error bars represent 95% confidence intervals, $n = 3$, with significance determined by one-way ANOVA with post-processing to correct for multiple comparisons. The overall *P*-value for this statistical model is indicated. Comparisons not labelled with asterisks were not statistically different. (**D**) Same as (**C**), except error bars represent s.e.m., $n = 3$. (**E**) A GST-pulldown was performed to compare binding of purified ΔN17-Arf1 (preloaded with GDP or GTP) to either the GST–FBE domain construct or GST alone. Arf1 was detected with anti-Arf1 antibody and the GST proteins were detected by Ponceau staining. (**F**) Arf1-dependent liposome pelleting was performed using a different batch of Folch liposomes. Occasionally, liposome batches bound proteins more weakly; we took advantage of one such batch to measure Arf1-dependent binding. Before adding exomer constructs to the '+Arf1' experimental condition, Arf1 was loaded with GTP in the presence of liposomes. Error bars represent s.e.m.; significance was determined using a two-tailed *t*-test, $n = 3$. Figure source data can be found with the Supplementary data.

indistinguishable from full-length GFP–Chs5 (Figure 7A; Supplementary Figure 7A).

Of all the truncation constructs we tested, the ΔN construct (GFP–Chs5(51–658)) most closely resembled the intact complex, exhibiting substantial TGN localization in addition to partial delocalization to the cytoplasm (Figure 7A). Full localization of the ΔN construct to the TGN was not restored by the fusion of an unrelated dimerization domain (GST) to the N-terminus (Supplementary Figure 7B), indicating that the Chs5 N-terminus has a role in TGN localization beyond simple dimerization, perhaps by positioning the two halves of the dimer in a particular orientation. Neither the Chs5 helix that interacts with the ChAPs (GFP–Chs5(51–80)), nor the FBE domain (GFP–Chs5(74–299) localized to the TGN (Figure 7A and B). The FBE domain did occasionally localize to non-TGN punctae (Figure 7B), the significance of which are unclear.

The isolated N-terminus (GFP–Chs5(1–55)), while mostly cytoplasmic, localized very faintly to the TGN (Figure 7A). TGN localization of the Chs5 N-terminus was significantly enhanced by an N-terminal GST fusion (Figure 7A, 'GST–N-terminus'). As the exomer crystal structure suggested that the N-terminus might interact with ChAP proteins *in trans*, we considered the possibility that the GST–N-terminus construct

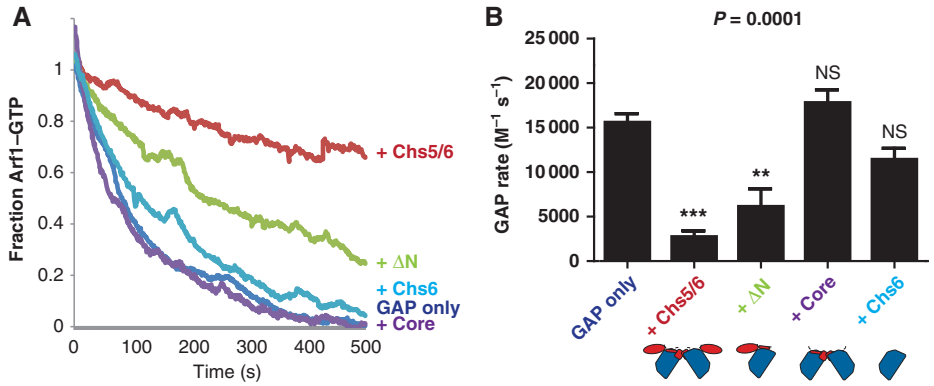

Figure 6 Exomer inhibits the ArfGAP activity of the Age2 GAP domain. (**A**) Tryptophan fluorescence assay to determine GAP rates of the Age2 GAP domain acting on Arf1–GTP either alone or in the presence of various exomer constructs (the same constructs as in Figure 6). Shown are averaged, normalized fluorescence traces. Before time = 0, Folch liposomes were first loaded with 0.5 μM Arf1–GTP, and purified exomer construct (or buffer control) was added to 0.25 μM. At time = 0, the GAP domain of Age2 was added to 0.50 μM. (**B**) Average GAP rates were calculated for the experiment in (**A**). Error bars represent 95% confidence intervals, $n \geqslant 3$, and significance was determined by one-way ANOVA with post-processing to correct for multiple comparisons. The overall *P*-value for the statistical analysis is indicated.

was aided in localizing to the TGN by an interaction with the ChAP proteins in cells. We therefore examined localization in cells additionally lacking all four ChAP genes (*bch1*Δ *bch2*Δ *bud7*Δ *chs5*Δ *chs6*Δ cells). We confirmed that wild-type Chs5 localized correctly to punctae in the absence of ChAPs (Trautwein *et al*, 2006), although we observed a faint cytosolic haze (Figure 7C) not visible in the presence of the ChAPs. The GST–N-terminus construct was significantly delocalized to the cytoplasm in the absence of the ChAPs (Figure 7C) relative to its localization in cells with intact ChAPs (Figure 7A), though very faint punctae were still visible. This indicates that the localization of the Chs5 N-terminus to the TGN depends strongly on the presence of the ChAPs.

The exomer core construct (GFP–Chs5(1–79)) also partially co-localized with Sec7 (Figure 7A). This was more clearly observed with a longer exposure time, which revealed TGN and cytoplasmic localization as well as localization to non-TGN puncta and occasional localization to the limiting vacuolar membrane (Figure 7B). Thus, loss of the FBE domain results in a partial mislocalization phenotype, and suggests that the ChAP proteins aid in localization of exomer to intracellular membranes, but interaction between the FBE domain and Arf1 provides specific targeting to the TGN.

We observed that the localization of the ΔN construct in cells lacking the ChAPs was completely cytoplasmic (Figure 7C), in contrast to the significant TGN localization we observed in the presence of the ChAPs (Figure 7A). This result confirms that the FBE domain is not sufficient for TGN localization in the absence of both the N-terminal dimerization domain and the membrane-binding affinity provided by the ChAP protein partner.

The localization data correlate well with the results of the *in vitro* assays, indicating that Arf1 binding by the FBE domain is required for proper exomer localization *in vivo*; ChAP protein binding to membranes (and cargo) also plays a significant role in localization. The data signify an additive effect, in which loss of any one of these interactions perturbs the localization of exomer to the TGN.

Discussion

Cargo adaptors are the primary machinery for sorting proteins in the secretory and endocytic pathways. Much of what is known about the structure and function of cargo adaptors is based on the COPI, COPII, and clathrin trafficking pathways; comparatively little is known about how other cargo adaptors function. This study provides new insights into the molecular architecture of a distinct cargo adaptor, exomer. The structure reveals a domain with unexpected structural resemblance to the appendage domains of other cargo adaptors, and our results establish that this FBE domain plays a critical role in localization of exomer to the TGN by binding directly to Arf1. To our knowledge, there are no previous examples of either a FN3 domain or a BRCT domain binding to a GTPase; the FBE domain is therefore a novel GTPase-binding domain.

Vesicle coat proteins are known to regulate the GTP cycle of their cognate G-proteins. In the case of the COPII coat, the Sec23 subunit itself functions as a GAP, and its activity is stimulated by the Sec31 subunit (Yoshihisa *et al*, 1993; Antonny *et al*, 2001). The COPI coat stimulates the GAP activity of ArfGAP proteins, likely by forming a tripartite complex with the GAP catalytic domain and the GTPase (Goldberg, 1999; Yu *et al*, 2012). The C-terminal non-catalytic regions of ArfGAPs also interact with the appendage domain of the COPI subunit γ-COP, providing an additional stimulatory interaction (Watson *et al*, 2004; Kliouchnikov *et al*, 2009; Schindler *et al*, 2009). We found that exomer inhibits GAP activity, likely by competing with ArfGAP for binding to Arf1. The GAP assay results confirmed the critical role of the FBE domain for Arf1 binding.

The GTPase cycle of Arf1 and related GTPases is intimately connected with vesicle biogenesis. Arf1 must remain GTP-bound long enough to recruit cargo adaptors, which recruit cargo and trigger assembly of the vesicle coat. Although somewhat controversial, GTP hydrolysis has been shown to be required for vesicle scission (Bielli *et al*, 2005), and is certainly necessary at some point in the life cycle of the vesicle. Our demonstration that exomer inhibits GAP-induced

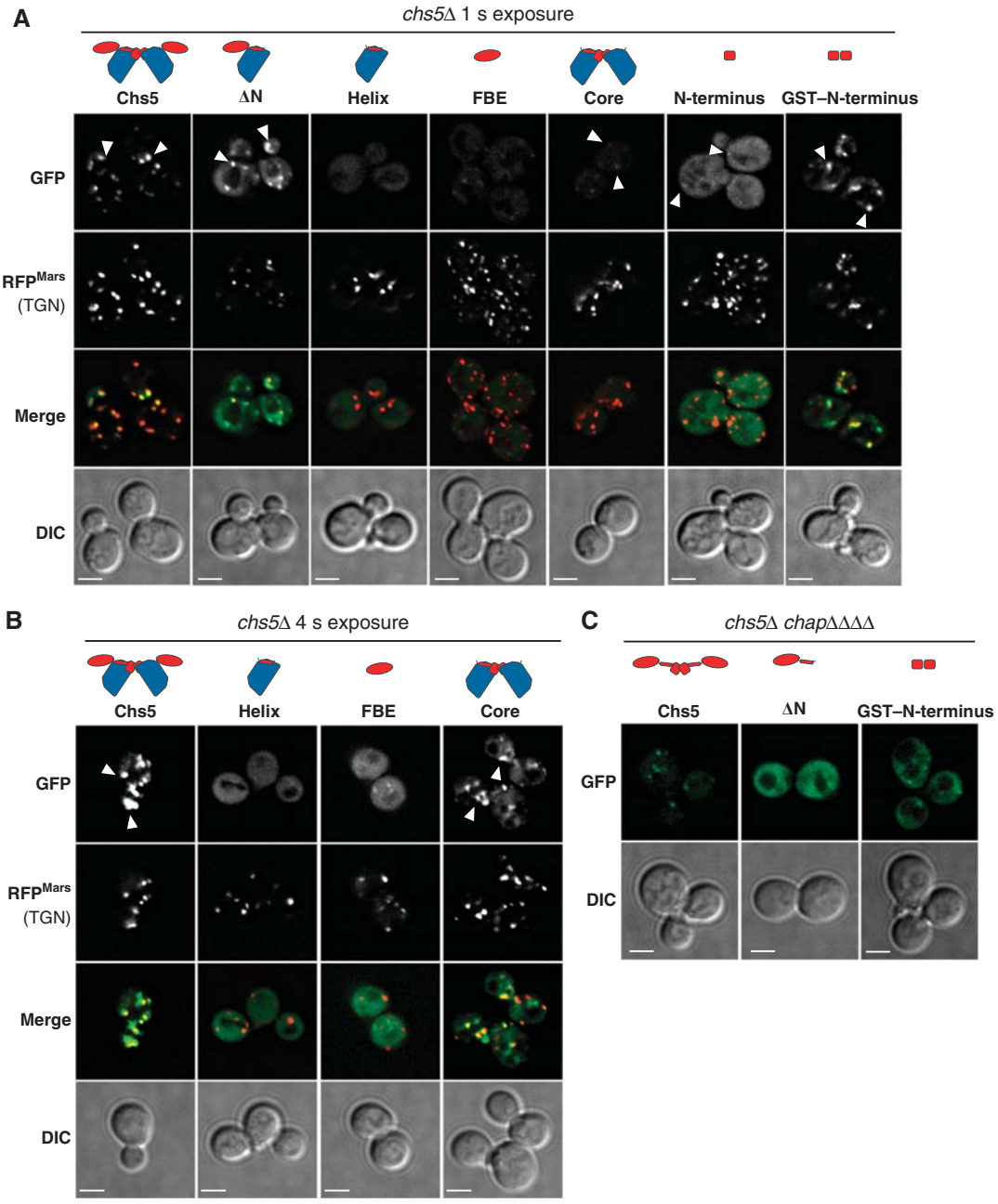

Figure 7 Multiple domains are involved in localization of exomer to the TGN. (**A**) Plasmids expressing GFP-tagged Chs5 constructs were introduced into *chs5*Δ *SEC7-RFP*^{Mars} cells (CFY885) and the cells were imaged. A single deconvolved focal plane is shown at equivalent light levels for each construct. Arrowheads indicate example punctae that co-localize with Sec7. Construct names and corresponding plasmids: 'Chs5' = GFP–Chs5(1–299); 'ΔN' = GFP–Chs5(51–658); 'Helix' = GFP–Chs5(51–80); 'FBE' = GFP–Chs5(74–299); 'Core' = GFP–Chs5(1–79); 'N-terminus' = GFP–Chs5(1–55); 'GST–N-terminus' = GST–GFP–Chs5(1–55). Scale bar, 2 μm. (**B**) Same as in (**A**), except using a 4-s exposure time in the green channel. Scale bar, 2 μm. (**C**) Plasmids expressing GFP-tagged Chs5 constructs were introduced into *bch1*Δ *bch2*Δ *bud7*Δ *chs5*Δ *chs6*Δ cells (CFY994) and the cells were imaged. Scale bar, 2 μm.

GTP hydrolysis indicates that exomer might play a direct role in controlling the GTP cycle of Arf1 during vesicle biogenesis. We speculate that during early stages of vesicle formation, exomer prevents premature Arf1–GTP hydrolysis through the action of the FBE domain, but during later stages of vesicle formation the inhibitory effect is relieved, perhaps by an increased local concentration of ArfGAP that is able to out-compete the FBE domain, thus triggering hydrolysis of Arf1-bound GTP.

We found that Chs6 is the primary component of the Chs5/6 complex that binds directly to membranes. This supports the postulated role of the ChAP proteins in binding to membrane-proximal sorting signals in the cytoplasmic domains of transmembrane cargo. The data at present are not sufficient to discern precisely how exomer binds membranes. Given the flexible linkage between the exomer core complex and the FBE domain, there remain a number of possibilities for the orientation of exomer relative to the

membrane surface that would allow for simultaneous binding of the ChAP to the membrane surface and the FBE domain to membrane-bound Arf1. Future determination of the structure of exomer bound to Arf1 may be necessary to establish exactly how exomer binds membranes.

Based on the functional interaction with the ubiquitously conserved Arf1 GTPase and the resemblance to helical solenoid structures found in other trafficking proteins, it is possible that exomer represents an evolutionarily ancient example of a cargo adaptor. Alternatively, exomer may be a highly specialized cargo adaptor that has convergently evolved the ability to be regulated by Arf1. To our knowledge, Chs5 (and its orthologues in other species) is the only protein with a BRCT domain that is not localized to the nucleus. BRCT domains are virtually always found as tandem arrays in proteins. An interesting twist of evolution has resulted in the pairing of BRCT and FN3 domains for a GTPase-binding module.

Materials and methods

Plasmids, strains, and antibodies

See Supplementary Tables 3 and 4 for a list of plasmids and yeast strains used. Yeast strains were created using standard techniques (Longtine *et al*, 1998). The *CHS5* gene we used as a source for all constructs was derived from the SEY6210 yeast strain. The SEY6210 Chs5 ORF sequence differs, in both sequence and length, from that of the S288C yeast strain used for the published genomic sequence, including one amino-acid difference in the fragment we used for crystallization (Ser at residue 271 instead of Asn). The Arf1 antibody was a gift from Randy Schekman.

Microscopy

Cells were grown in synthetic dropout media and imaged in log phase ($OD_{600} \sim 0.5$). Live cells were imaged at room temperature on one of two microscopes. For Figures 1 and 7; Supplementary Figures 1 and 7, we used a DeltaVision RT wide-field deconvolution microscope (Applied Precision). Images were deconvolved using SoftWoRx 3.5.0 software (Applied Precision). For Figure 2F and Supplementary Figure 7A, we used a laser-illuminated, CSU-X spinning disk (Intelligent Imaging Innovations) controlled by Slidebook 5.0 (Intelligent Imaging Innovations). Images were further processed in Adobe Photoshop, adjusting only min/max light levels for clarity, and using equivalent processing for all images within an experiment. Exposure times for the GFP, RFP, and DIC channels were 1, 0.5, and 0.1 s, respectively, unless otherwise noted in the figure panel.

Protein expression and purification

Recombinant *Saccharomyces cerevisiae* Chs5 (residues 1–299) and Chs6–6xHis were co-expressed from a plasmid (pJP13) derived from the pETDuet-1 vector, transformed into Rosetta-2 (DE3) *E. coli* cells (Novagen). Cells were harvested by centrifugation and resuspended in lysis buffer (450 mM KOAc, 10% glycerol, 50 mM HEPES pH 7.4, 20 mM imidazole pH 8, 10 mM BME) prior to lysis by sonication. Affinity purification using Ni-NTA agarose resin (Qiagen) was followed by anion exchange (MonoQ; GE Healthcare), hydrophobic interaction (Phenyl HP; GE Healthcare), and gel filtration chromatography (Superose 6; GE Healthcare). The final purified protein was concentrated to 40 mg/ml in a buffer of 150 mM NaCl, 10 mM HEPES pH 7.4, and 2 mM DTT.

Other exomer constructs and mutants were produced by a similar procedure. Yeast Age2 GAP domain (residues 4–133) and ΔN17-Arf1 were expressed as constructs with a TEV protease cleavable N-terminal 6xHis-tag. After nickel purification, the His-tag was removed by TEV protease and the protein was further purified by gel filtration chromatography (Superdex 200; GE Healthcare). Recombinant myristoylated yeast Arf1 was purified following a previously published protocol (Ha *et al*, 2005). GST fusions were purified following the protocol recommended by the glutathione resin manufacturer (GE Healthcare), using PBS buffer.

Crystallization and structure determination

The Chs5/6 complex was crystallized by the hanging drop vapour diffusion method from drops containing a 2:1 mixture of protein: precipitant (350 mM KCl and 1 mM DTT). Crystals were cryoprotected in a solution consisting of the precipitant plus 30% (v/v) glycerol. The crystals belong to the $P6_322$ space group with unit cell dimensions $a = b = 166$ Å and $c = 264$ Å. Heavy atom derivatives were obtained by addition of 10 mM thimerosal or 10 mM cadmium to the cryoprotectant solution. Crystals were soaked at room temperature for 10 min (Joyce *et al*, 2010), then frozen in $N_2(l)$. Diffraction data were collected at CHESS (Cornell High Energy Synchrotron Source) beamline A1 and NSLS (National Synchrotron Light Source) beamline X25. Data were processed using HKL-2000 (Otwinowski and Minor, 1997) and experimental phases were determined by multiple isomorphous replacement with anomalous scattering (MIRAS). Heavy atom sites and experimental phases were calculated from each of the two derivative crystals separately using SHELX (Sheldrick, 2008). The two sets of phases were then combined, extended, and subjected to density modification using PHENIX (Adams *et al*, 2010). The structure was built manually using Coot (Emsley *et al*, 2010) in multiple iterations alternating with refinement in PHENIX. The N-terminal region of Chs5 (residues 1–49) was modelled as poly-alanine due to poor electron density. The residue number assignments of this region of the model were chosen based on secondary structure prediction. It was not obvious from the electron density whether this region of Chs5 was connected to the Chs5 molecule bound to the nearest Chs6, or was instead connected to the Chs5 molecule bound to a more distal Chs6 related by crystal symmetry (see text, shown in Figure 3C and D and compare Figure 1 with Supplementary Figure 3). Structural images were generated with PyMOL.

Sedimentation velocity and stokes radius analysis

Molecular weights of the purified complexes were determined by combined analysis of experimentally determined sedimentation velocity and Stokes radius (Erickson, 2009). A mixture of each Chs5/6 exomer complex and standards was loaded at the top of a 5-ml continuous 5–20% sucrose gradient and centrifuged for 10 h at 330 000 *g*. In all, 150 µl fractions were collected from the bottom of the gradient and analysed by SDS–PAGE, and the Chs5/6 peak was compared with that of the standards to determine the sedimentation coefficient. The Stokes radius of the Chs5/6 exomer complex was calculated by comparison of elution volume from a gel filtration column to the elution volumes of calibration standards. Native molecular weight was calculated using the formula

$$\mathrm{MW_{native}} = 4205\ \mathrm{Daltons\,nm^{-1}\,Sv^{-1}} * R_s(\mathrm{in\ nm}) * S(\mathrm{in\ Sv})$$

Size-exclusion chromatography-coupled MALS

Purified protein was separated using a WTC-030S5 column (Wyatt Technology) equilibrated in buffer (20 mM HEPES pH 7.5, 150 mM NaCl, 1 mM DTT) prior to injection. The column was coupled to a static 18-angle light scattering detector (DAWN HELEOS-II) and a refractive index detector (Optilab T-rEX) (Wyatt Technology). Data analysis was carried out using the program ASTRA.

Preparation of synthetic liposomes

Unilamellar liposomes were generated from a mixture of lipids, using either Folch fraction I (Sigma), or a synthetic mixture approximating the endogenous TGN lipid composition determined in a published lipidomics study (Klemm *et al*, 2009; Richardson *et al*, 2012), with 1% DiR near-infrared dye (Avanti Polar Lipids) to aid in visualization and quantification of lipids. Following vacuum drying, lipid films were hydrated in 20 mM HEPES pH 7.4, 150 mM KOAc, followed by extrusion through 100 nm filters to generate liposomes. Due to some batch-to-batch variation, each figure panel represents data collected using a single batch of liposomes (the same batch was used for Figure 5C and D).

Arf1-dependent liposome binding assay

The liposome flotation assay was performed essentially as described (Matsuoka *et al*, 1998; Wang *et al*, 2006; Richardson *et al*, 2012). TGN-like liposomes were incubated with 6 µg Arf1 in the presence of 625 µM EDTA and 125 µM GMPPNP or GDP for 1 h. The exchange reaction was stopped with 2.5 mM $MgCl_2$, and the

liposome–Arf1 mixtures were incubated for 1 h with 6 μg of purified exomer construct. Liposomes were separated from unbound protein by sucrose gradient ultracentrifugation: sucrose was added to the binding reaction to 1 M, layered with 0.75 M sucrose buffer followed by sucrose-free buffer, and spun at 100 000 r.p.m. for 20 min at 20°C in a TLA-100 ultracentrifuge rotor. The top layer was collected and bound proteins assessed by SDS–PAGE, with loading normalized for lipid recovery as measured by DiR fluorescence.

Liposome pelleting assay

A binding reaction consisting of 2 μg of protein with or without 300 μM liposomes in 40 μl total volume of HKM buffer (20 mM HEPES pH 7.4, 150 mM KOAc, and 1 mM $MgCl_2$) was incubated at room temperature for 15 min. The samples were spun at 15 000 *g* for 10 min at 4°C. The supernatant was removed, a sample was taken for gel analysis, and the pellet was resuspended in 40 μl 1 × SDS sample buffer/HKM. The samples were heated at 55°C for 15 min with frequent vortexing. The samples were run on SDS–PAGE and stained with IRDye (Li-COR) before scanning on an Odyssey imager (Li-COR). Band intensities were determined using Odyssey software to determine the relative amount of protein in the pellet (P) or supernatant (S) fractions. The background-subtracted percentage of protein pelleted was calculated using the formula:

$$[P_{\text{liposomes.}}/(P_{\text{liposomes}} + S_{\text{liposomes.}})] - [P_{\text{no liposomes}}/(P_{\text{no liposomes}} + S_{\text{no liposomes}})].$$

Tryptophan fluorescence GAP assay

The nucleotide-bound state of Arf was monitored by a native tryptophan fluorescence assay (297.5 nm excitation, 340 nm emission) (Antonny *et al*, 1997) performed at 30°C. HKM buffer, 200 μM Folch liposomes, 0.5 μM Arf1, 100 μM GTP, and 2 mM EDTA were added sequentially and the reaction was allowed to incubate until Arf1 was completely loaded with GTP, as monitored by the corresponding increase in fluorescence signal. $MgCl_2$ was then added to 5 mM. Exomer constructs were added to 0.25 μM, followed by the addition of the GAP domain of Age2 to 0.5 μM, which marked $t = 0$ for the experiment. Traces were fit to a one-phase exponential decay curve using GraphPad Prism to determine the GAP rate for each experiment. Experimental traces were not included in subsequent analysis if the R^2 value for the curve fitting was below 0.95 (0.90 for experiments with the intact Chs5/6 complex, due to difficulty with curve fitting at slower rates). The averaged raw fluorescence traces shown in Figure 6A were normalized before averaging.

Accession number

The coordinates and structure factors have been deposited in the Protein Data Bank with the accession code 4GNS.

Supplementary data

Supplementary data are available at *The EMBO Journal* Online (http://www.embojournal.org).

Acknowledgements

We thank the laboratories of Scott Emr and Tony Bretscher for use of their microscopes, as well as to Chris Stefan and Bret Judson for technical assistance with microscopy. We thank Damien Garbett and the laboratory of Tony Bretscher for assistance with sucrose velocity gradient analysis. We thank Laura Byrnes in the laboratory of Holger Sondermann with assistance with MALS. We thank the laboratory of Steve Ealick for the gift of heavy atom compounds. We thank Robyn Barfield, Tony Bretscher, Scott Emr, and Holger Sondermann for critical reading of the manuscript. We thank Randy Schekman for encouragement and advice, and Harvey McMahon for a helpful discussion regarding the FBE domain. We are grateful for the use of beamline A1 at CHESS, and beamline X25 at the NSLS. We received expert technical advice from Marian Szebenyi at CHESS A1 and Annie Heroux at NSLS X25. CHESS was supported by the National Science Foundation and the National Institutes of Health/National Institute of General Medical Sciences under NSF award DMR-0225180, using the Macromolecular Diffraction at CHESS (MacCHESS) facility, which was supported by award RR-01646 from the National Institutes of Health, through its National Center for Research Resources. NSLS was supported principally by the Offices of Biological and Environmental Research and of Basic Energy Sciences of the US Department of Energy, and by the National Center for Research Resources of the National Institutes of Health Grant number P41RR012408. We were supported by startup funds to JCF from Cornell University, and by NIH Training Grant (T32GM07273) awards to JEP and AMS.

Author contributions: JEP, BCR, AMS, and JCF designed the experiments. JEP, BCR, and AMS performed the experiments. JEP, BCR, and JCF prepared the manuscript.

Conflict of interest

The authors declare that they have no conflict of interest.

References

Adams PD, Afonine PV, Bunkoczi G, Chen VB, Davis IW, Echols N, Headd JJ, Hung LW, Kapral GJ, Grosse-Kunstleve RW, McCoy AJ, Moriarty NW, Oeffner R, Read RJ, Richardson DC, Richardson JS, Terwilliger TC, Zwart PH (2010) PHENIX: a comprehensive Python-based system for macromolecular structure solution. *Acta Crystallogr D Biol Crystallogr* **66**(Pt 2): 213–221

Antonny B, Huber I, Paris S, Chabre M, Cassel D (1997) Activation of ADP-ribosylation factor 1 GTPase-activating protein by phosphatidylcholine-derived diacylglycerols. *J Biol Chem* **272:** 30848–30851

Antonny B, Madden D, Hamamoto S, Orci L, Schekman R (2001) Dynamics of the COPII coat with GTP and stable analogues. *Nat Cell Biol* **3:** 531–537

Ashkenazy H, Erez E, Martz E, Pupko T, Ben-Tal N (2010) ConSurf 2010: calculating evolutionary conservation in sequence and structure of proteins and nucleic acids. *Nucleic Acids Res* **38**(Web Server issue): W529–W533

Barfield RM, Fromme JC, Schekman R (2009) The exomer coat complex transports Fus1p to the plasma membrane via a novel plasma membrane sorting signal in yeast. *Mol Biol Cell* **20:** 4985–4996

Bi X, Corpina RA, Goldberg J (2002) Structure of the Sec23/24-Sar1 pre-budding complex of the COPII vesicle coat. *Nature* **419:** 271–277

Bi X, Mancias JD, Goldberg J (2007) Insights into COPII coat nucleation from the structure of Sec23-Sar1 complexed with the active fragment of Sec31. *Dev Cell* **13:** 635–645

Bielli A, Haney CJ, Gabreski G, Watkins SC, Bannykh SI, Aridor M (2005) Regulation of Sar1 NH2 terminus by GTP binding and hydrolysis promotes membrane deformation to control COPII vesicle fission. *J Cell Biol* **171:** 919–924

Bonifacino JS, Glick BS (2004) The mechanisms of vesicle budding and fusion. *Cell* **116:** 153–166

Bonifacino JS, Lippincott-Schwartz J (2003) Coat proteins: shaping membrane transport. *Nat Rev Mol Cell Biol* **4:** 409–414

Brohawn SG, Leksa NC, Spear ED, Rajashankar KR, Schwartz TU (2008) Structural evidence for common ancestry of the nuclear pore complex and vesicle coats. *Science* **322:** 1369–1373

Bulawa CE (1992) CSD2, CSD3, and CSD4, genes required for chitin synthesis in Saccharomyces cerevisiae: the CSD2 gene product is related to chitin synthases and to developmentally regulated proteins in Rhizobium species and Xenopus laevis. *Mol Cell Biol* **12:** 1764–1776

Choi WJ, Sburlati A, Cabib E (1994) Chitin synthase 3 from yeast has zymogenic properties that depend on both the CAL1 and the CAL3 genes. *Proc Natl Acad Sci USA* **91:** 4727–4730

Chuang JS, Schekman RW (1996) Differential trafficking and timed localization of two chitin synthase proteins, Chs2p and Chs3p. *J Cell Biol* **135:** 597–610

Collins BM, McCoy AJ, Kent HM, Evans PR, Owen DJ (2002) Molecular architecture and functional model of the endocytic AP2 complex. *Cell* **109:** 523–535

Collins BM, Praefcke GJ, Robinson MS, Owen DJ (2003) Structural basis for binding of accessory proteins by the appendage domain of GGAs. *Nat Struct Biol* **10:** 607–613

De Matteis MA, Luini A (2008) Exiting the Golgi complex. *Nat Rev Mol Cell Biol* **9:** 273–284

De N, Navarro MV, Wang Q, Krasteva PV, Sondermann H (2010) Biophysical assays for protein interactions in the Wsp sensory system and biofilm formation. *Methods Enzymol* **471:** 161–184

Donaldson JG, Jackson CL (2011) ARF family G proteins and their regulators: roles in membrane transport, development and disease. *Nat Rev Mol Cell Biol* **12:** 362–375

Edeling MA, Mishra SK, Keyel PA, Steinhauser AL, Collins BM, Roth R, Heuser JE, Owen DJ, Traub LM (2006) Molecular switches involving the AP-2 beta2 appendage regulate endocytic cargo selection and clathrin coat assembly. *Dev Cell* **10:** 329–342

Emsley P, Lohkamp B, Scott WG, Cowtan K (2010) Features and development of Coot. *Acta Crystallogr D Biol Crystallogr* **66**(Pt 4): 486–501

Erickson HP (2009) Size and shape of protein molecules at the nanometer level determined by sedimentation, gel filtration, and electron microscopy. *Biol Proced Online* **11:** 32–51

Glick BS, Nakano A (2009) Membrane traffic within the Golgi apparatus. *Annu Rev Cell Dev Biol* **25:** 113–132

Goldberg J (1999) Structural and functional analysis of the ARF1-ARFGAP complex reveals a role for coatomer in GTP hydrolysis. *Cell* **96:** 893–902

Ha VL, Thomas GM, Stauffer S, Randazzo PA (2005) Preparation of myristoylated Arf1 and Arf6. *Methods Enzymol* **404:** 164–174

Heldwein EE, Macia E, Wang J, Yin HL, Kirchhausen T, Harrison SC (2004) Crystal structure of the clathrin adaptor protein 1 core. *Proc Natl Acad Sci USA* **101:** 14108–14113

Hoffman GR, Rahl PB, Collins RN, Cerione RA (2003) Conserved structural motifs in intracellular trafficking pathways: structure of the gammaCOP appendage domain. *Mol Cell* **12:** 615–625

Ismail SA, Vetter IR, Sot B, Wittinghofer A (2010) The structure of an Arf-ArfGAP complex reveals a Ca2 + regulatory mechanism. *Cell* **141:** 812–821

Jackson LP, Kelly BT, McCoy AJ, Gaffry T, James LC, Collins BM, Honing S, Evans PR, Owen DJ (2010) A large-scale conformational change couples membrane recruitment to cargo binding in the AP2 clathrin adaptor complex. *Cell* **141:** 1220–1229

Joyce MG, Radaev S, Sun PD (2010) A rational approach to heavy-atom derivative screening. *Acta Crystallogr D Biol Crystallogr* **66**(Pt 4): 358–365

Kent HM, McMahon HT, Evans PR, Benmerah A, Owen DJ (2002) Gamma-adaptin appendage domain: structure and binding site for Eps15 and gamma-synergin. *Structure* **10:** 1139–1148

Klemm RW, Ejsing CS, Surma MA, Kaiser HJ, Gerl MJ, Sampaio JL, de Robillard Q, Ferguson C, Proszynski TJ, Shevchenko A, Simons K (2009) Segregation of sphingolipids and sterols during formation of secretory vesicles at the trans-Golgi network. *J Cell Biol* **185:** 601–612

Kliouchnikov L, Bigay J, Mesmin B, Parnis A, Rawet M, Goldfeder N, Antonny B, Cassel D (2009) Discrete determinants in ArfGAP2/3 conferring Golgi localization and regulation by the COPI coat. *Mol Biol Cell* **20:** 859–869

Lee C, Goldberg J (2010) Structure of coatomer cage proteins and the relationship among COPI, COPII, and clathrin vesicle coats. *Cell* **142:** 123–132

Longtine MS, McKenzie 3rd A, Demarini DJ, Shah NG, Wach A, Brachat A, Philippsen P, Pringle JR (1998) Additional modules for versatile and economical PCR-based gene deletion and modification in Saccharomyces cerevisiae. *Yeast* **14:** 953–961

Martin-Garcia R, de Leon N, Sharifmoghadam MR, Curto MA, Hoya M, Bustos-Sanmamed P, Valdivieso MH (2011) The FN3 and BRCT motifs in the exomer component Chs5p define a conserved module that is necessary and sufficient for its function. *Cell Mol Life Sci* **68:** 2907–2017

Matsuoka K, Orci L, Amherdt M, Bednarek SY, Hamamoto S, Schekman R, Yeung T (1998) COPII-coated vesicle formation reconstituted with purified coat proteins and chemically defined liposomes. *Cell* **93:** 263–275

Mossessova E, Bickford LC, Goldberg J (2003) SNARE selectivity of the COPII coat. *Cell* **114:** 483–495

Ortiz D, Novick PJ (2006) Ypt32p regulates the translocation of Chs3p from an internal pool to the plasma membrane. *Eur J Cell Biol* **85:** 107–116

Otwinowski Z, Minor W (1997) Processing of X-ray Diffraction Data Collected in Oscillation Mode. *Methods Enzymol* **276:** 307–326

Owen DJ, Vallis Y, Noble ME, Hunter JB, Dafforn TR, Evans PR, McMahon HT (1999) A structural explanation for the binding of multiple ligands by the alpha-adaptin appendage domain. *Cell* **97:** 805–815

Owen DJ, Vallis Y, Pearse BM, McMahon HT, Evans PR (2000) The structure and function of the beta 2-adaptin appendage domain. *EMBO J* **19:** 4216–4227

Poon PP, Nothwehr SF, Singer RA, Johnston GC (2001) The Gcs1 and Age2 ArfGAP proteins provide overlapping essential function for transport from the yeast trans-Golgi network. *J Cell Biol* **155:** 1239–1250

Richardson BC, McDonold CM, Fromme JC (2012) The Sec7 Arf-GEF is recruited to the trans-Golgi network by positive feedback. *Dev Cell* **22:** 799–810

Roncero C, Valdivieso MH, Ribas JC, Duran A (1988) Isolation and characterization of Saccharomyces cerevisiae mutants resistant to Calcofluor white. *J Bacteriol* **170:** 1950–1954

Saci A, Cantley LC, Carpenter CL (2011) Rac1 regulates the activity of mTORC1 and mTORC2 and controls cellular size. *Mol Cell* **42:** 50–61

Sanchatjate S, Schekman R (2006) Chs5/6 complex: a multiprotein complex that interacts with and conveys chitin synthase III from the trans-Golgi network to the cell surface. *Mol Biol Cell* **17:** 4157–4166

Santos B, Duran A, Valdivieso MH (1997) CHS5, a gene involved in chitin synthesis and mating in Saccharomyces cerevisiae. *Mol Cell Biol* **17:** 2485–2496

Santos B, Snyder M (1997) Targeting of chitin synthase 3 to polarized growth sites in yeast requires Chs5p and Myo2p. *J Cell Biol* **136:** 95–110

Santos B, Snyder M (2003) Specific protein targeting during cell differentiation: polarized localization of Fus1p during mating depends on Chs5p in Saccharomyces cerevisiae. *Eukaryot Cell* **2:** 821–825

Schekman R, Orci L (1996) Coat proteins and vesicle budding. *Science* **271:** 1526–1533

Schindler C, Rodriguez F, Poon PP, Singer RA, Johnston GC, Spang A (2009) The GAP domain and the SNARE, coatomer and cargo interaction region of the ArfGAP2/3 Glo3 are sufficient for Glo3 function. *Traffic* **10:** 1362–1375

Sheldrick GM (2008) A short history of SHELX. *Acta Crystallogr A* **64:** 112–122

Trautwein M, Schindler C, Gauss R, Dengjel J, Hartmann E, Spang A (2006) Arf1p, Chs5p and the ChAPs are required for export of specialized cargo from the Golgi. *EMBO J* **25:** 943–954

Valdivieso MH, Mol PC, Shaw JA, Cabib E, Duran A (1991) CAL1, a gene required for activity of chitin synthase 3 in Saccharomyces cerevisiae. *J Cell Biol* **114:** 101–109

Wang CW, Hamamoto S, Orci L, Schekman R (2006) Exomer: A coat complex for transport of select membrane proteins from the trans-Golgi network to the plasma membrane in yeast. *J Cell Biol* **174:** 973–983

Watson PJ, Frigerio G, Collins BM, Duden R, Owen DJ (2004) Gamma-COP appendage domain - structure and function. *Traffic* **5:** 79–88

Yoshihisa T, Barlowe C, Schekman R (1993) Requirement for a GTPase-activating protein in vesicle budding from the endoplasmic reticulum. *Science* **259:** 1466–1468

Yu X, Breitman M, Goldberg J (2012) A structure-based mechanism for Arf1-dependent recruitment of coatomer to membranes. *Cell* **148:** 530–542

Zahner JE, Harkins HA, Pringle JR (1996) Genetic analysis of the bipolar pattern of bud site selection in the yeast Saccharomyces cerevisiae. *Mol Cell Biol* **16:** 1857–1870

Zanolari B, Rockenbauch U, Trautwein M, Clay L, Barral Y, Spang A (2011) Transport to the plasma membrane is regulated differently early and late in the cell cycle in Saccharomyces cerevisiae. *J Cell Sci* **124**(Pt 7): 1055–1066

Ziman M, Chuang JS, Tsung M, Hamamoto S, Schekman R (1998) Chs6p-dependent anterograde transport of Chs3p from the chitosome to the plasma membrane in Saccharomyces cerevisiae. *Mol Biol Cell* **9:** 1565–1576